

Aerodynamic Effect on Stability and Lift Characteristics of an Elevated Sedan Car

Amrutheswara Krishnamurthy and Suresh Nagesh

PES University, Bangalore-560085, Karnataka, India

ABSTRACT

There is a strong interaction between air and vehicle components. Aerodynamics plays a significant role in a vehicle's fuel efficiency. The contact patch load between the tire and road is directly related to the vehicle load. In this research, the lift forces generated due to the additional wing attached to the car model with different spans and heights of the wing location from the car body is considered for study. The loads due to change in Angle of Attack (AOA) and their effect on the tire loads are studied. The upward vertical force produced from aerodynamic loads reduces the wheel load of

the car virtually. A tire's coefficient of friction would decrease with upward vertical force. This balance load implies that a lightweight car would make more efficient use of its tires than a heavier car. ANSYS Fluent is used for the Computational Fluid Dynamics (CFD) study. The validation of airflow characteristics, lift and drag forces from simulations are done with wind tunnel testing data. Varying the angle of attack, wingspan, height between the car and the wing's lower surface, one can increase the capacity of the payload by 10% or fuel efficiency by 10% to 20%.

KEYWORDS: Aerodynamics, Navier Stoke equation, Nozzle effect, Car-wing, Drag, Lift.

Introduction

Aerodynamics plays a vital role in the fuel efficiency and stability of the vehicle. The airfoil in sedan cars are utilized to create adequate stability; however, the fuel efficiency decreases. Stability is required to steer the vehicle at high speeds. While the vehicle is moving with constant velocity, the aerodynamic forces and the tire contact patch almost remain constant. More the contact patch, more stability and less fuel efficiency, and vice versa. The entire vehicle load transfer to the road via the contact patch between the road and tire. The vertical load [5] includes lift force and downward force. Force on each tire is proportional to vertical load and significantly influences the longitudinal and lateral forces

The idea to use a wing or Airfoil fitted to the Car at the Center is to make use of the space between the Car's upper surface and the lower surface of the Airfoil to cause a Venturi nozzle effect [11]. The difference between the lower pressure on the Wing's top surface and high pressure at the upper surface of the Car's body creates upward lift force. The Wing attached starts from the center position of the Car and extended until the rear end of the Car.

In the study performed by Ahmed et al., the ground vehicle type of bluff body [1] was analyzed. In an open wind tunnel test section, pressure measurements and force measurements were done. The drag comes from the slant [6], [24], and the vertical base surface of the rear end. Numerical investigations by Emmanuel Guilmineau [8], [9] show that the angle of the rear window has significant

effects on the characteristics of the wake flow. The drag always affects the fuel consumption and minimizes with the proper aerodynamic shape of the vehicle. The work by W Hucho [10] shows that a vehicle's aerodynamic shape is resisting the airflow in highways, and pressure drag contributes to total drag as a major, which consumes about 50% of the vehicle's fuel at highway speeds. The low level of drag loads and increased lift loads adds to the fuel efficiency. In race car aerodynamics [12], [29], the lift forces in -ve z-direction pushes the Car downward with the negative angle of attack.

It is vitally important to design new era cars with good aerodynamic shape [13], [15] to reduce fuel consumption as much as possible. If it is an electric vehicle [17], increasing the range to avoid frequent charging on highways is very advantageous. The engine's efficiency, idle time reduction, the torque required to drive the wheel at a higher speed would also affect the fuel efficiency. This current study focused on the aerodynamic forces. This type of car design uses air stream as additional fuel, renewable energy.

The authors in the current paper studied the Car attached to a wing at the top surface of the Car and studied the aerodynamic forces. The novelty of the research is without increasing the coefficient of drag, with AOA less than 4 deg, lift forces are generated due to nozzle effect. The weight of the Car could be reduced virtually using the lift forces. The performed experiments and study revealed that increasing the wingspan increases the lift forces. The angle of attack is one of the parameters, and increasing the AOA, lift and drag forces significantly

increased. The contact patch loads calculated using the lift and drag forces generated show that loads on the tires decrease. These loads help to evaluate the lateral and longitudinal loads at the contact patch. These loads would help to design a liter vehicle and improve fuel efficiency.

Tire Load Interaction

The main forces acting at the tire-road contact patch are longitudinal forces [2], [7], [19] lateral forces, and self-alignment torque. The ratio gives the coefficient of friction

$$\mu = \frac{F_{tx}}{F_v} \quad \dots(1)$$

F_{tx} is the force in the X direction, F_v , the vertical load. Therefore, the ratio μ is friction coefficient [28] depends on tire slip resulting from contact patch due to vertical load.

In the Pacejka [21] tire model, lateral force and aligning torque are calculated based on slip angle and longitudinal force, mainly dependent on normal force F_z which is transferred to the tire, ignoring the camber angle.

The overall tire deflection estimates by the vertical load divided by the vertical stiffness. The Tire deflection, longitudinal force, lateral force, and slip are depending on the vertical load on the wheel. The vehicle's power must be equal to the power of the driving wheels.

Fig. 1 shows the general schematic diagram of six DOF vehicle models.

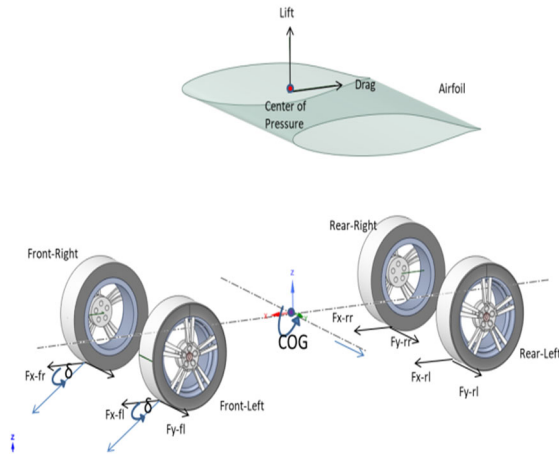


Fig. 1. The schematic diagram of six DOF vehicle model.

The basic equations describing the vehicle dynamics [4], [18] are as follows.

$$a_x = \frac{1}{m} [(F_{x_{fl}} + F_{x_{fr}}) \cos \delta - ((F_{y_{fl}} + F_{y_{fr}}) \sin \delta) + (F_{x_{rl}} + F_{x_{rr}})] \quad \dots(2)$$

$$a_y = \frac{1}{m} [(F_{x_{fl}} + F_{x_{fr}}) \sin \delta + ((F_{y_{fl}} + F_{y_{fr}}) \cos \delta) + (F_{y_{rl}} + F_{y_{rr}})] \quad \dots(3)$$

$$\frac{dr}{dt} = \frac{1}{I_{zz}} [(F_{x_{fl}} + F_{x_{fr}}) * a * \sin \delta + ((F_{y_{fl}} + F_{y_{fr}}) * a * \cos \delta) - (F_{y_{rl}} + F_{y_{rr}}) * b - ((F_{x_{fl}} + F_{x_{fr}}) \cos \delta * twf * 0.5 - ((F_{x_{rl}} - F_{x_{rr}}) * twr * 0.5)] \quad \dots(4)$$

$$a_x = \dot{v}_x - v_y r \quad \dots(5)$$

$$a_y = \dot{v}_y + v_x r \quad \dots(6)$$

Where

v Speed of the Car

a Acceleration

r Yaw rate

F Force

δ Steering Angle

The indices refer to wheels

FL Front left

FR Front right

RL Rear left

RR Rear right

a Distance from CoG to the front axel

b Distance from CoG to the rear axel

twf Front track width

twr Rear track width

I_{zz} Inertia around z-axis for the yaw movement

$$F_{wheels} = \frac{T_{Engine\ torque} * i_{Gear\ ratio} * \eta_{efficiency}}{r_d r_{dynamic}} = F_{Total\ Force} \quad \dots(7)$$

$$= F_{Air\ drag} + F_{Rolling\ resistance} + F_{Inertia} + F_{Slope} \quad \dots(8)$$

As the vehicle speed increases, the load on the tires, rolling resistance, and drag forces [3] also increase. The drag mainly depends on the frontal design and area of the Car. Adding the Wing does not increase the frontal area significantly; however, it depends on the angle of attack. An increase in AOA results in higher drag force and less lift force.

$$F_{Air\ drag} = \frac{C_d \text{coefficient drag} * S * \rho_{air} * \theta^2}{2} \quad \dots(9)$$

$$F_{Rolling\ resistance} = m(\text{Kerb weight} + \text{Passengers}) * g * f_{rr} * \cos \alpha \quad \dots(10)$$

f_{rr} is coefficient of rolling force, let us assume Slope angle

$$\alpha = 0 \quad F_{Inertia} = m(\text{Kerb weight} + \text{Passengers}) * a * v \quad \dots(11)$$

Under constant acceleration, the term $F_{Inertia}$ ignored.

The lift force is not going to affect the frontal area calculations.

$$F_{lift} = \frac{C_l \text{coefficient lift} * S * \rho_{air} * \theta^2}{2} \quad \dots(12)$$

The basic dynamic equation has the mass m in the denominator, which reduces due to the lift force.

The contact patch load for the front wheel is given by

$$F_{Contact\ Patch\ load} = \frac{m * g * (1 - \frac{CG}{WB})}{2} + F_s - \frac{F_{lift}}{4} + \frac{F_{Air\ drag + COG}}{4} \quad \dots(13)$$

Where F_s is the vertical suspension load, WB is the wheelbase. Drag loads due to Airfoil are transferred to the CG to calculate loads at the tire contact patch. As a result, the total load decreases due to the lift loads, reducing F_z loads and reducing the torque required to drive the wheels.

A setup for measuring the aerodynamic forces in a wind tunnel consists of a mechanism suitable for rigidly fixing the car model's position with the desired orientation up to ± 30 degrees relative to the airstream. The wind tunnel facility has a maximum jet velocity speed of up to

45 m/s, and it is of an open-return design. The cross-sectional dimension of the nozzle area where the test model was placed is 600mm square. It has a glass window for visual observation of flow phenomenon. Wind tunnel equipped with a platform-type external strain gauge balance on which the model is to be mounted. All forces and moments were measured using a 3-component balance system. The model is fixed at the center position in this wind tunnel configuration, as shown in Fig. 3.

CFD

(a) **Meshing details:** The water-tight geometry has been used in the analysis from the Ansys space claim. The CFD mesh is generated using the following method. More fine resolution meshes were used around the vehicle. A body of influence is created around the vehicle, and a finer mesh size of 4 mm is used. Similarly, one more body of influence is created around the Airfoil with a small mesh to capture the flow separation and study the lift forces. Inflation layers are created around the Airfoil with the growth rate of 1.2. about the CFD model has 60 millions elements and 10 millions nodes for the purpose of analysis. Mesh independent study has been performed prior to finalizing this mesh type and size. Polyhedral mesh is used for discretization.

Computational fluid dynamics (CFD) analysis [8], [14], [25], [26], [27] is carried out to compare the results. The turbulence model k- ω SST model [16] is used in analyzing the flow characteristics of this computational problem. The default boundary conditions used in the CFD [17], [20], [22], [23] analysis.

The Turbulence Kinetic Energy model is calculated as shown in equation 14.

$$\frac{\partial k}{\partial t} + U_j \frac{\partial k}{\partial x_j} = P_k - \beta k \omega + \frac{\partial}{\partial x_j} [(v + \sigma_{v_T}) \frac{\partial k}{\partial x_j}] \dots(14)$$

(b) **NACA 66(2)015:** Symmetrical NACA 66(2)-015 Airfoil is attached to the car body. NACA 662-015 Airfoil has greater laminar flow than the 4 and 5 series, and this type of Airfoil has low drag. The minimum pressure location is at 0.6 chord length. CFD analysis is done to study the lift generated with various angles of attacks ANNEXURE – B:

The Y ordinate matches the centerline of the car body. The X ordinate of the Center of the pressure of the Wing measures the same as the Center of Gravity's (CG) Y ordinate. Due to this, there won't be any moment acting on the front and rear wheel axel. Only lift force reduces the load virtually on the car body, which reduces the overall load acting on the tires. The gap between the Airfoil and the Car's top surface is maintained so that the airflow is not affected, as shown in

Fig. 4. Only the Wing's angle of incidence is modified, where the Car is parallel to the x-axis.

Table 1 presents the coordinates used for the NACA 662015 symmetrical airfoil. At the same time, importing the coordinate points into the Fluent,

adding one more point with Y ordinate as 0 to create a closed-end for the Airfoil as shown in the table. Units are in mm.

TABLE 1.

The coordinates of the NACA 662015 airfoil are attached to the car body.

X_Cord	Y_Cord	X_Cord	Y_Cord
0.00	0.0000	95.00	-0.5660
0.50	1.1220	90.00	-1.4800
0.75	1.3433	85.00	-2.5300
1.25	1.6753	80.00	-3.5980
2.50	2.2353	75.00	-4.2987
5.00	3.1000	75.00	-4.2987
7.50	3.7813	70.00	-5.5760
10.00	4.3580	65.00	-6.3720
15.00	5.2860	60.00	-6.9593
20.00	5.9953	55.00	-7.2833
25.00	6.5433	50.00	-7.4500
30.00	6.9560	45.00	-7.4953
35.00	7.2500	40.00	-7.4300
40.00	7.4300	35.00	-7.2500
45.00	7.4953	30.00	-6.9560
50.00	7.4500	25.00	-6.5433
55.00	7.2833	20.00	-5.9953
60.00	6.9593	15.00	-5.2860
65.00	6.3720	10.00	-4.3580
70.00	5.5760	7.50	-3.7813
75.00	4.2987	5.00	-3.1000
80.00	3.5980	2.50	-2.2353
85.00	2.5300	1.25	-1.6753
90.00	1.4800	0.75	-1.3433
95.00	0.5660	0.50	-1.1220
100.00	0.0000		

Test Model

In this study, a 1:18 scaled car model used is the Porche Panamera model, and technical details were taken from the Techart [30] and Porche website [31]. The model used in the windtunnel lab is a die-cast metal miniature scaled model but a very detailed, available in the market. The CAD data of the same was replicated using CATIA for the CFD analysis. The model is attached with the Airfoil with different wingspans at different heights.

The following parameters were studied.

Starting with a 100mm wingspan increased up to 300 mm in steps of 50mm. (100mm, 150mm, 200mm, 250mm, and 300mm) in total, five wings were fixed to the car body.

The distance between the Car's top surface and the Wing's lower surface for the aerodynamic effect is studied. Initially, it was 25 mm and then increased the height to 25mm, i.e., 25mm, 50mm, and 75mm. The angle of incidence varied as 0°, 5°, 8°, 15° degrees. However, the

Airfoil has a stalling angle of 16°; hence the study is limited to 15°.



Fig. 2. The Wind tunnel test facility.



Fig. 3. The Car body with the Airfoil attached in the wind tunnel test.

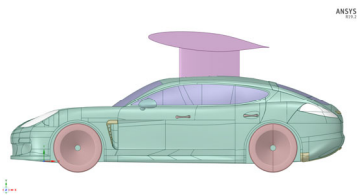


Fig. 4. Geometrical model of the Car body with the Airfoil attached.

Fig. 3 shows the scaled model in the wind tunnel lab with the Wing fixed on the top.

Fig. 4 shows the geometrical model used in the analysis.

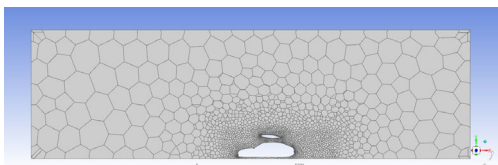


Fig. 5. The CFD model of the Car body with the Airfoil attached.



Fig. 6. The Pressure plot of the CFD model of Car.

Fig. 5 shows the polyhedral mesh with symmetrical modeling. Fig. 6 shows the pressure plot from the CFD simulation.

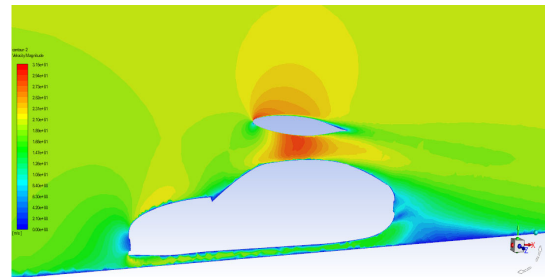


Fig. 7. The Velocity plot of the CFD model of Car.

Fig. 7 shows the velocity plot from the same simulation where drag remains the same, but the lift force is improved.

Results and Discussion

(a) **Wind Tunnel Results:** Results obtained from the CFD study and results from the wind tunnel tests are discussed in detail here. The graph shown in Fig. 8 depicts that an increase in the wingspan increases the lift force for a given airflow velocity. In this experiment, AOA is kept constant at 5° degrees, and the wingspan is varied, and the airflow velocity increased from 1m/s to 20m/s.

Table 2 presents the lift forces measured in the WindTunnel test with the different wingspans attached to the car body where the angle of attack is kept constant.

TABLE 2.

The Wind tunnel test result values of the car model with airfoil attached

Velocity (m/s)	100mm Lift (N)	150mm Lift (N)	200mm Lift (N)	250mm Lift (N)
1.14	0.03	0.02	0.03	0.01
2.3	0.03	0.02	0.01	0.09
4.15	0.06	0.05	0.12	0.24
5.76	0.12	0.13	0.29	0.37
7.3	0.17	0.25	0.48	0.85
9.07	0.25	0.35	0.77	1.01
10.7	0.34	0.46	1.04	1.81
12.2	0.48	0.61	1.37	1.91
13.01	0.52	0.72	1.61	2.22
13.9	0.64	0.92	1.78	2.52
14.76	0.69	1.09	1.95	2.79
15.9	0.88	1.16	2.21	3.12
16.5	1.05	1.29	2.45	3.40
17	1.14	1.36	2.71	3.80
18	1.21	1.46	2.91	4.23
19	1.29	1.56	3.04	4.43

The results show in Fig. 9 are the results of the experiments done in the wind tunnel for the Car attached with the Wing, of span 100mm and Wing alone analyzed using the CFD software Fluent. The investigation was carried out by varying the air velocity from 1m/s to 20 m/s keeping the angle of attack at 5 deg. This lift force increase shows that the nozzle effect obtained from the lift is higher than the only Wing lift forces.

The graphs in Fig. 10 depict the relationship between the Wing attached to the Car and the aerodynamic forces. Observed that when the angle of attack is less than 10°, an upward force is generated and increases with the angle of attack. Here in this experiment Wing span used is 200mm, and varied the angle of attack is 5 and 8 degrees. The lift loads increase 22% when the angle of attack is changed from 5 degrees to 8 degrees, with the vehicle's speed is around 70kmph.

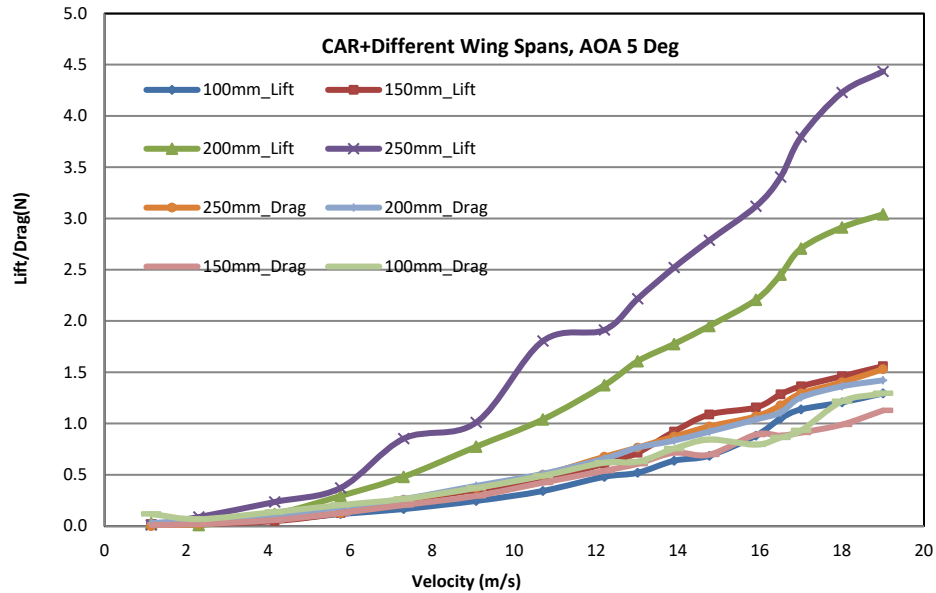


Fig. 8. Lift vs. velocities for symmetric Airfoil attached to CAR with different wingspans.

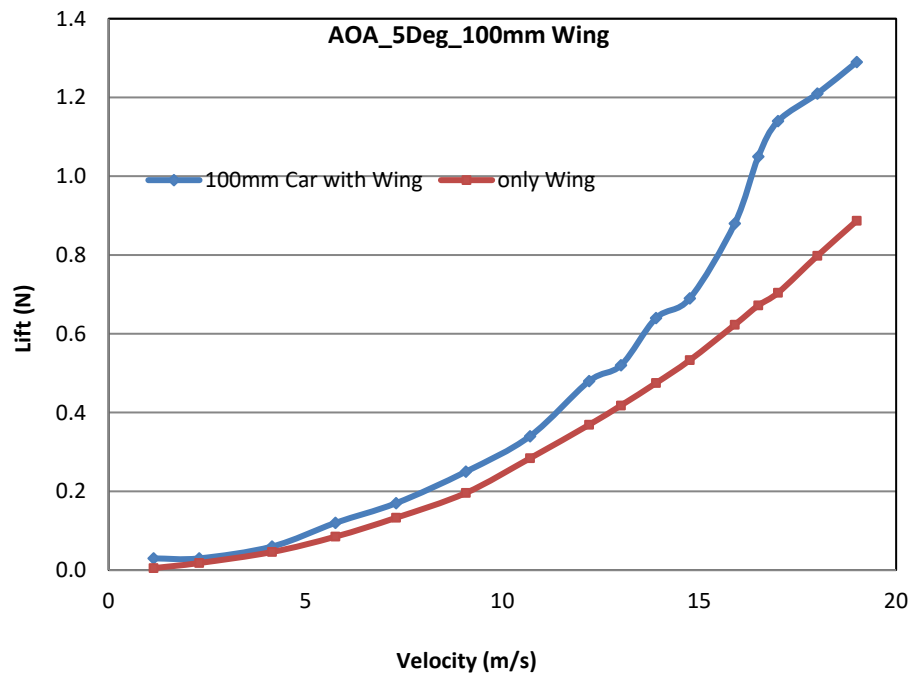


Fig. 9. Lift vs. velocities for Airfoil attached to CAR and Only Wing without a car.

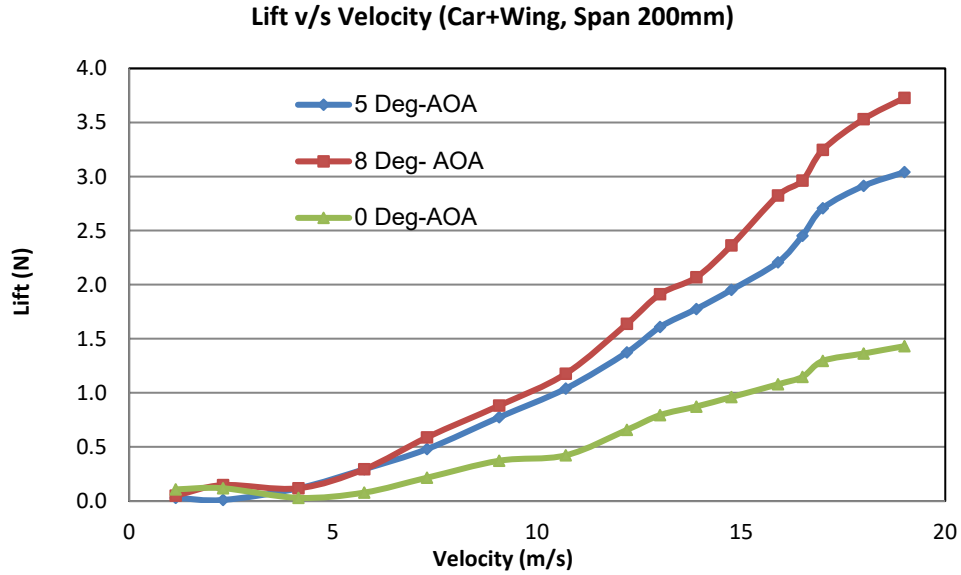


Fig. 10. Lift vs. velocities for symmetric Airfoil attached to CAR with different angles of attack.

Further, Fig. 11 shows that the lift forces generated decrease when the height between the Wing's lower surface and the car body increases. In this experiment, height is varied from 25 mm to 50 mm. and velocity from 1m/s to 40 m/s. The distance from the ground level is increased by 24% approximately. The lift loads generated decreased by 8.3% at the speed of 40m/s with the angle of attack 8 degrees. This curve shows that the nozzle effect reduces, and hence the total lift generated decreases as the height increases. The results shown in this curve are related to wind tunnel experiment results. The height increased to 75mm, and the results are much more similar

to 50mm; hence, the optimum height is essential to utilize the nozzle effect.

CFD Results validation

We used high-performance computing machines for the CFD analysis. The results obtained from CFD analysis and Wind tunnel experiments are compared here in Fig. 12. The CFD results for 3D Wingspan 250mm with 8 Deg of AOA and Wind Tunnell results showed an error of $\pm 1.5\%$ in Wind tunnel results.

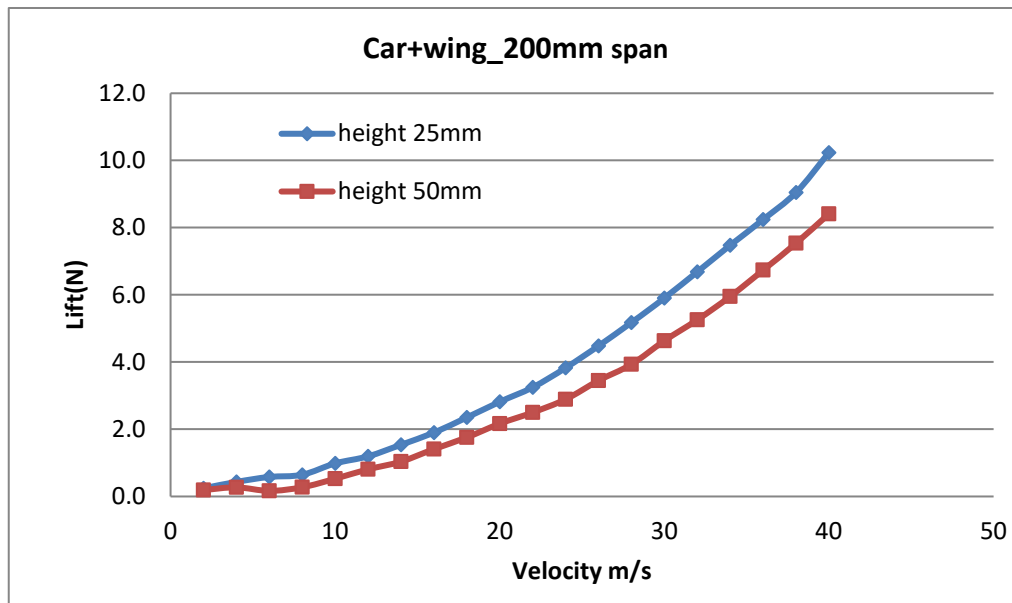


Fig. 11. Lift vs. velocities for symmetric Airfoil attached to CAR with a different height between Car and the Airfoil.

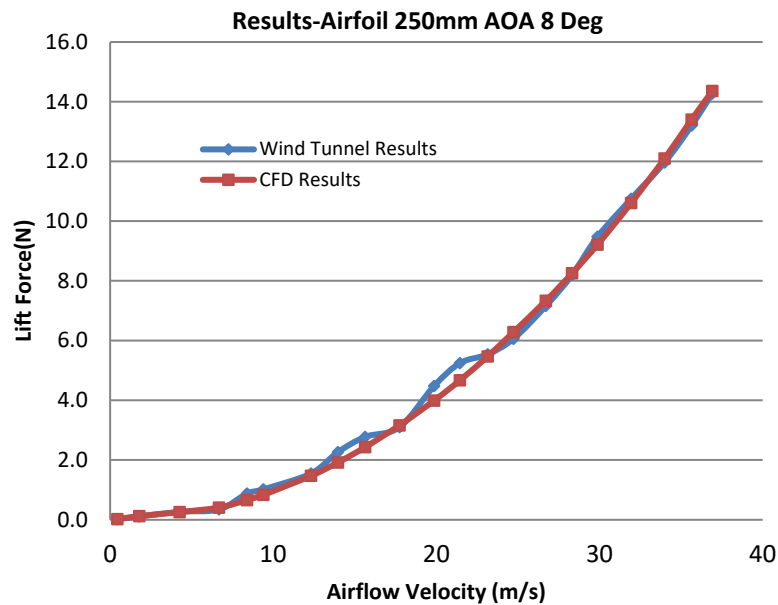


Fig. 12. Error in Measurements, Lift vs. velocities for Airfoil with wingspan 250mm and AOA 8 Deg.

Experiments were performed and compared using the wind tunnel to study the behavior with different wingspans attached to the car body. The aerodynamic lift loads from the Airfoil to the load balance measurement are transferred through the car body, as depicted in Fig. 3. The Car is mounted to strain gauge balance at the Center of the car bottom and through which aerodynamic loads are transferred and measured. This mounting depicts that a car with the airfoil attachment could pass the lift forces to wheel axels. Longitudinal forces and lateral forces are related directly as per equation 13. As F_z (vertical) loads reduce, the fuel efficiency increases; however, the lift is directly proportional to the square of the vehicle's velocity. The more the lift force, the more the vehicle gets into the unstable mode. Hence study has been done up to 130kmph of airspeed in the wind tunnel test. In general increase in lift and a decrease in drag are shown to increase fuel efficiency.

Since the Car model used in this study is a 1:18 scaled model. The NACA 662015 airfoil of a 200mm wingspan is up-scaled to normal dimensions, i.e.18, and with that, the wingspan measures to be 3.6m. Wingspan was analyzed using CFD, which shows that it generates 2775N lift force at 36m/s airspeed and 5° of AOA. After converting this lift force into kg, it is almost 282kg, virtually reducing weight. The car models of this size have a Kerb weight of approximately 2450kg. Hence the airlifted weight would be 11.5%. In turn, reduction in fuel consumption per 100km = $282 \times (0.4/100) = 1.1$ L/100km.

Summary/Conclusions

A Car fitted with a simple wing on the top surface with different wingspans and AOA is studied in this paper. The measured load depicts the increase in wingspan influences the lift loads. Computed contact

patch loads due to virtually decreased weight, aerodynamic drag, and lift loads show that the loads on each tire reduced. The Venturi nozzle effect generates lift force at zero degrees of angle of attack and no drag. The lift loads reduce the loads on the contact patch, which adds to the 10% fuel efficiency.

Acknowledgement

Sunshine Measuring Instruments Pvt Ltd partially supported this research by providing the wind tunnel setup and the models. We are also grateful to Dr. TR Sitharam and Dr. Prabhu for their guidance.

References

- [1] Ahmed, S., Ramm, G., & Faltin, G. (1984). Some Salient Features Of The Time-Averaged Ground Vehicle Wake. SAE Technical Paper Series, 473–503.
<https://doi.org/10.4271/840300>
- [2] Baffet, G., Charara, A., & Lechner, D. (2009). Estimation of vehicle sideslip, tire force and wheel cornering stiffness. Control Engineering Practice, 17(11), 1255–1264.
<https://doi.org/10.1016/j.conengprac.2009.05.005>
- [3] Bayındırlı, C., & Çelik, M. (2018). The Experimentally and Numerically Determination Of The Drag Coefficient Of A Bus Model. International Journal of Automotive Engineering and Technologies, 7(3), 117–123.
<https://doi.org/10.18245/ijaet.486409>
- [4] Department of Automatic Control Lund Institute of Technology, & Gerard, M. (2006). Tire-Road Friction Estimation Using Slip-based Observers (ISRN LUTFD2/TFRT--5771--SE).
<http://lup.lub.lu.se/luur/download?func=downloadFile&recordId=8847816&fileId=8859385>

- [5] Dominy, R. G. (1992). Aerodynamics of Grand Prix Cars. Proceedings of the Institution of Mechanical Engineers, Part D: Journal of Automobile Engineering, 206(4), 267–274. https://doi.org/10.1243/pime_proc_1992_206_18_7_02
- [6] Gaylard, A., Kabanovs, A., Jilesen, J., Kirwan, K., & Lockerby, D. (2017). Simulation of rear surface contamination for a simple bluff body. Journal of Wind Engineering and Industrial Aerodynamics, 165, 13–22. <https://doi.org/10.1016/j.jweia.2017.02.019>
- [7] Gillespie, T. D. (1992). Fundamentals of Vehicle Dynamics. SAE International.
- [8] Guilmineau, E. (2014). Numerical Simulations of Flow around a Realistic Generic Car Model. SAE International Journal of Passenger Cars - Mechanical Systems, 7(2), 646–653. <https://doi.org/10.4271/2014-01-0607>
- [9] Guilmineau, E. (2018). Effects of Rear Slant Angles on the Flow Characteristics of the Ahmed Body by IDDES Simulations. SAE Technical Paper Series, 001–0010. <https://doi.org/10.4271/2018-01-0720>
- [10] Hucho, W., & Sovran, G. (1993). Aerodynamics of Road Vehicles. Annual Review of Fluid Mechanics, 25(1), 485–537. <https://doi.org/10.1146/annurev.fl.25.010193.002413>
- [11] Huminic, A., Huminic, G., & Soica, A. (2012). Study of aerodynamics for a simplified car model with the underbody shaped as a Venturi nozzle. International Journal of Vehicle Design, 58(1), 15. <https://doi.org/10.1504/ijvd.2012.045927>
- [12] Katz, J. (2006). AERODYNAMICS OF RACE CARS. Annual Review of Fluid Mechanics, 38(1), 27–63. <https://doi.org/10.1146/annurev.fluid.38.050304.092016>
- [13] Kim, I., & Chen, H. (2010). Reduction of aerodynamic forces on a minivan by a pair of vortex generators of a pocket type. International Journal of Vehicle Design, 53(4), 300. <https://doi.org/10.1504/ijvd.2010.034103>
- [14] Mansour, H., Afify, R., & Kassem, O. (2020). Three-Dimensional Simulation of New Car Profile. Fluids, 6(1), 8. <https://doi.org/10.3390/fluids6010008>
- [15] Matsumoto, D., Kiewat, M., Haag, L., & Indinger, T. (2018). Online Dynamic Mode Decomposition Methods for the Investigation of Unsteady Aerodynamics of the DrivAer Model (First Report). International Journal of Automotive Engineering, 9(2), 64–71. https://doi.org/10.20485/jsaeijae.9.2_64
- [16] Menter, F. R. (1994). Two-equation eddy-viscosity turbulence models for engineering applications. AIAA Journal, 32(8), 1598–1605. <https://doi.org/10.2514/3.12149>
- [17] Nabil, T., Helmy Omar, A. B., & Mohamed Mansour, T. (2020). Experimental Approach and CFD Simulation of Battery Electric Vehicle Body. International Journal of Fluid Mechanics & Thermal Sciences, 6(2), 36. <https://doi.org/10.11648/j.ijfmts.20200602.11>
- [18] Milliken, W. F. (1995). [Race Car Vehicle Dynamics (Premiere Series)] [Author: William F. Milliken] [December, 1995]. SAE International.
- [19] Olson, B., Shaw, S., & Stepa'n, G. (2003). Nonlinear Dynamics of Vehicle Traction. Vehicle System Dynamics, 40(6), 377–399. <https://doi.org/10.1076/vesd.40.6.377.17905>
- [20] Romijn, T., Hendrix, W., & Donkers, M. (2017). Modeling and Control of a Radio-Controlled Model Racing Car. IFAC-PapersOnLine, 50(1), 9162–9167. <https://doi.org/10.1016/j.ifacol.2017.08.1726>
- [21] Ružinskias, A., & Sivilevičius, H. (2017). Magic Formula Tyre Model Application for a Tyre-Ice Interaction. Procedia Engineering, 187, 335–341. <https://doi.org/10.1016/j.proeng.2017.04.383>
- [22] Strangfeld, C., Wieser, D., Schmidt, H. J., Wozidlo, R., Nayeri, C., & Paschereit, C. (2013). Experimental Study of Baseline Flow Characteristics for the Realistic Car Model DrivAer. SAE Technical Paper Series, 2342–2350. <https://doi.org/10.4271/2013-01-1251>
- [23] Targosz, M., Skarka, W., & Przystalka, P. (2018). Model-Based Optimization of Velocity Strategy for Lightweight Electric Racing Cars. Journal of Advanced Transportation, 2018, 1–20. <https://doi.org/10.1155/2018/3614025>
- [24] Tunay, T., Sahin, B., & Ozbolat, V. (2014). Effects of rear slant angles on the flow characteristics of Ahmed body. Experimental Thermal and Fluid Science, 57, 165–176. <https://doi.org/10.1016/j.exptthermflusci.2014.04.016>
- [25] Varney, M., Passmore, M., Wittmeier, F., & Kuthada, T. (2020). Experimental Data for the Validation of Numerical Methods: DrivAer Model. Fluids, 5(4), 236. <https://doi.org/10.3390/fluids5040236>
- [26] Varshney, H. (2017). Aerodynamic Drag Reduction of Tractor-Trailer using Wishbone Type Vortex Generators. International Journal for Research in Applied Science and Engineering Technology, V(IX), 1833–1846. <https://doi.org/10.22214/ijraset.2017.9266>
- [27] Viswanathan, H. (2021). Aerodynamic performance of several passive vortex generator configurations on an Ahmed body subjected to yaw angles. Journal of the Brazilian Society of

Mechanical Sciences and Engineering, 43(3), 25–31.

<https://doi.org/10.1007/s40430-021-02850-8>

- [28] Wang, R., & Wang, J. (2013). Tire–road friction coefficient and tire cornering stiffness estimation based on longitudinal tire force difference generation. *Control Engineering Practice*, 21(1), 65–75. <https://doi.org/10.1016/j.conengprac.2012.09.009>
- [29] Zhang, X., Toet, W., & Zerihan, J. (2006). Ground Effect Aerodynamics of Race Cars. *Applied Mechanics Reviews*, 59(1), 33–49. <https://doi.org/10.1115/1.2110263> Haslam, E. *Shikimic Acid Metabolism and Metabolites*, John Wiley & Sons: New York, 1993.
- [30] Techart for the Panamera models. (n.d.). Techart. <https://www.techart.de/en/models/panamera/techart-for-970/>
- [31] Porsche Panamera 4S. (n.d.). Porsche AG - Dr. Ing. h.c. F. Porsche AG. <https://www.porsche.com/international/models/panamera/panamera-models/panamera-4s/>

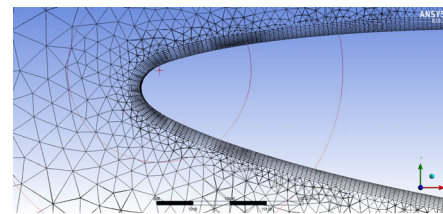
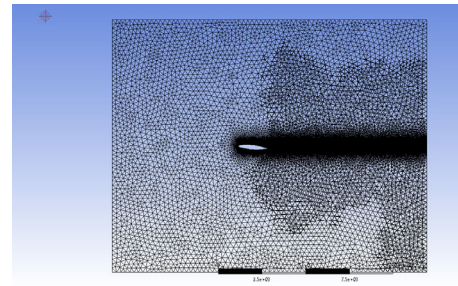
ANNEXURE – A:

Boundary conditions

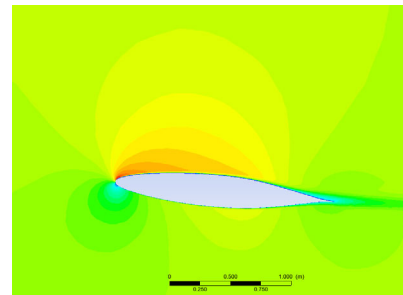
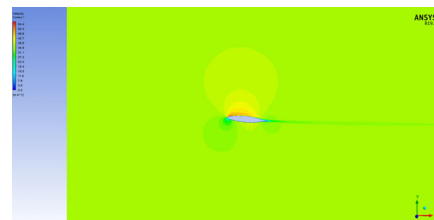
Velocity Inlet	
Velocity Specification Method	Magnitude and direction
Velocity Magnitude	30 m/s
X-Component of flow direction	1
Specification Method	Intensity and Viscosity Ratio
Back Flow Turbulent Intensity (%)	5
Back Flow Turbulent Viscosity Ratio	10
Reference Values	
Compute from	Inlet
Area (m ²)	0.25617m ²
Density (kg/m ³)	1.225
Viscosity (kg/m-s)	1.7894E-05
Reference Zone	
Solution Methods	
Scheme	Coupled
Gradient	Least Square Cell Based
Pressure	Second Order
Momentum	Second Order Upwind
Turbulent Kinetic Energy	Second Order Upwind
Specific Dissipation Rate	Second Order Upwind

ANNEXURE – B:

CFD analysis of the NACA662015



CFD Mesh



Velocity Contour

Address correspondence to : Mr. Amrutheswara Krishnamurthy, Research Scholar, PES University, Bangalore-560085, Karnataka, India
 Email: amruthisac@gmail.com
 Phone: 09900523702
